



Applying spaceborne reflectivity measurements for calculation of the solar ultraviolet radiation at ground level

P. N. den Outer¹, A. van Dijk¹, H. Slaper¹, A. V. Lindfors², H. De Backer³, A. F. Bais⁴, U. Feister⁵, T. Koskela², and W. Josefsson⁶

¹National Institute for Public Health and the Environment, Bilthoven, The Netherlands

²Finnish Meteorological Institute, Helsinki, Finland

³Royal Meteorological Institute of Belgium, Uccle, Belgium

⁴Aristotle University of Thessaloniki, Thessaloniki, Greece

⁵Deutscher Wetterdienst, Lindenberg, Germany

⁶Swedish Meteorological and Hydrological Institute, Norrköping, Sweden

Correspondence to: P. N. den Outer (peter.den.outer@rivm.nl)

Received: 9 December 2011 – Published in Atmos. Meas. Tech. Discuss.: 4 January 2012

Revised: 6 November 2012 – Accepted: 16 November 2012 – Published: 10 December 2012

Abstract. Long-term analysis of cloud effects on ultraviolet (UV) radiation on the ground using spaceborne observations requires the use of instruments that have operated consecutively. The longest data record can be built from the reflectivity measurements produced by the instruments Total Ozone Mapping Spectrometers (TOMS) flown on Nimbus 7 from 1979 to 1992, TOMS on Earth Probe from 1996 to 2005, and the Ozone Monitoring Instrument (OMI) flown on EOS Aura since 2004. The reflectivity data produced by TOMS on Earth Probe is only included until 2002. A comparison is made with cloud effects inferred from ground-based pyranometer measurements at over 83 World Radiation Data Centre stations. Modelled UV irradiances utilizing the standard reflectivity are compared with measurements of UV irradiances at eight European low-elevation stations. The reflectivity data of the two TOMS instruments shows a consistent agreement, and the required corrections are of low percentage, i.e. 2–3%. In contrast, the reflectivity product of OMI requires correction of 7–10%, and a solar angle dependency therein is more pronounced. These corrections were inferred from a comparison with pyranometer data, and tested using the UV measurements. The average reduction of UV radiation due to clouds for all sites together indicates a small trend: a diminishing cloudiness, in line with ground-based UV observations. Uncorrected implementation of the reflectivity data would have indicated the opposite.

An optimal area was established for reflectivity data for the calculation of daily sums of UV radiation. It measures approximately 1.25° in latitudinal direction for square-shaped areas overhead the ground-based UV stations. Such an area can be traversed within 5 to 7 h at the average wind speeds found for the West European continent.

1 Introduction

The amount of ozone in the stratosphere and the presence of clouds are atmospheric properties that mostly determine the level of solar ultraviolet (UV) radiation at the Earth's surface. Long-term trends or changes in these particular atmospheric properties therefore have direct consequences for UV radiation exposure and hence, important implications for health and ecosystems (UNEP, 2010; WMO, 2011). To determine the transmission of solar radiation through the atmosphere, measuring the downwelling UV radiation with ground-based instruments that are facing up is an inherently more accurate approach than measuring reflections at the top of the atmosphere. However, only spaceborne instruments can capture the full regional- and global-scale effects owing to UV radiation exposure.

Long-term assessment of UV-radiation levels is required to evaluate effects of environmental change on UV-related health effects. It exceeds the life span of spaceborne

instruments. Therefore, these types of analyses will generally be based on data from instruments that have operated sequentially. This puts high demands not only on an absolute calibration but even more on the instrument-to-instrument comparability.

A minimal requirement to determine the ground-level UV radiation using spaceborne observations is access to total column ozone data and a cloud effect proxy. Improvements to the derived UV radiation levels can then be made by incorporating (local) ancillary data, e.g. spaceborne-retrieved or ground-based measured data on aerosols optical depth and snow cover, or profile information.

Total column ozone has been monitored continuously from space since the Total Ozone Mapping Spectrometer (TOMS) on NIMBUS 7 (N7) started in 1978, except for a data gap between 1993 and 1996. In the recent past, there were simultaneously operating instruments: TOMS on Earth Probe (EP), Global Ozone Monitoring Experiment (GOME) (Burrows et al., 1999), Scanning Imaging Absorption Spectrometer for Atmospheric Cartography (SCIAMACHY) (Bovensmann et al., 1999), Ozone Monitoring Instrument (OMI) (Levelt et al., 2006) and GOME-2 (<http://www.esa.int/esaME/gome-2.html>). Differences between the instruments exist in the number of overpasses per day, overpass times of the spacecrafts, and instrument properties like field of view, viewing angles, spectral resolution, wavelength range, etc. This leads to a variety of data products in addition to total column ozone that can be inferred from these instruments. Data products of the two TOMS instruments and OMI are accessible through the Ozone and Air Quality WebPages (ozoneaq.gsfc.nasa.gov). The Tropospheric Emission Monitoring Internet Service (www.temis.nl) gives links to SCIAMACHY, GOME and GOME-2 data products. Although not all instruments have daily global coverage, advanced data assimilation or “now casting” provides daily global coverage for all aforementioned instruments. In fact, data assimilation provides data every 6 h for GOME and SCIAMACHY (Eskes et al., 2003). As a result, a merged data set for the whole spaceborne observation period has been constructed for the total column ozone (Van der A et al., 2010).

Unfortunately, in contrast to total column ozone, spaceborne cloud products have a much lower uniformity. This could well be the consequence of cloud products often being an intermediate product in, for instance, trace gas retrievals. The variety in cloud products and the wavelength for which they have been derived make an assimilation difficult, and thereby long-term analysis of the UV radiation relevant to adverse and positive effects. Assimilation is also hampered by the much higher intrinsic spatial and temporal variability of clouds than that of total column ozone.

Many studies have demonstrated the ability (and limitations) of spaceborne measurements to assess the ground-level UV radiation (Eck et al., 1995; Herman et al., 1999; Kalliskota et al., 2000; Matthijsen et al., 2000; Krotkov et al., 2001; Kazantzidis et al., 2006; Arola et al., 2009; Kazadzis

et al., 2009). Cloud effects for summer periods derived from the International Satellite Cloud Climatology Project (ISCCP) data – cloud fraction and optical depth – perform a little worse than derived from the reflectivity (Matthijsen et al., 2000; Williams et al., 2004). Daily sums of UV irradiance using ISCCP data indicate a similarly good performance with respect to the standard deviations (Lindfors et al., 2009). Herman et al. (2009) made a long-term analysis of the Lambertian Equivalent Reflection (LER) data set on a global scale, also including data from the Sea-viewing Wide Field-of-view Sensor (Barnes et al., 2001). Diurnal variations were investigated showing that generally above-sea LER peaks in the morning, in contrast to LER over land, which peaks in the afternoon (Labow et al., 2011). Herman (2010) made a global analysis of the UV irradiance using 30 yr of satellite data, showing that zonal average UV irradiance has increased significantly since 1979, except for the equatorial band. Kleipool et al. (2008) constructed global climatology maps of the minimum LER using three years of OMI data and 23 wavelengths between 328 and 500 nm, and found good agreement with similar maps based on EP-TOMS (TOMS flown on Earth Probe) and GOME. Also typical features like higher reflectivity in open oceans, indicative of low phytoplankton levels, could be identified.

Building on the work of Matthijsen et al. (2000) and Williams et al. (2004), we make an assessment of the readily available reflectivity data from three consecutive operating instruments: N7-TOMS (TOMS flown on Nimbus 7), EP-TOMS, and OMI (flown on EOS Aura). We investigate how well daily sums of ground-level UV irradiance can be modelled by applying the reflectivity product, and focus on the differences between the three instruments in the determined cloud effects for UV irradiance. In contrast to most other studies, our focus is on cloud effect proxies for daily sums. The daily sums of UV radiation provide the potential daily exposure and are the building blocks for long-term assessments of UV radiation related health effects. Thus a good agreement of daily UV sums shall be our major interest.

Reflectivity data is the longest and most readily available data record and enables to perform these long-term studies required for UV radiation-related health issues in the first place. Secondly, the reflectivity data is close to an actual measurement and automatically incorporates the complexity of the cloud-scattered radiation. While non-radiative cloud parameters like cloud octas and cloud fraction need again an interpretation of their effect on the incoming (diffuse and direct) radiation.

A separation of the cloudless sky analysis and the effects of clouds is a simplification that has many practical advantages, and has led to well established approaches (see for review Calbó et al., 2005). Integration towards daily sums and the use of effective UV (spectral weighted wavelength integrated UV radiation) reduces the variability of the radiation and the need for detailed information of the atmospheric composition. The cloudless sky analysis can then be

Table 1. Versions, download location and date per reflectivity data set. Chronological information on version updates can be found on <http://toms.gsfc.nasa.gov/news/news.html>.

Data set satellite & instrument	Grid size (decimal degrees)	Used period	λ (nm)	Version ID used data sets	Download location (download date) Current location (creation date)
NIMBUS Nimbus 7 TOMS	1.0×1.25	1978 1993	331	L3, V8, NRT REFLECT GEN:04.119	DVD release (April 2004) ozoneaq.gsfc.nasa.gov/index.md * (April 2004)
EPTOMS Earth Probe TOMS	1.0×1.25	1996 2002	331	L3, V8, NRT REFLECT GEN: 04.116 V8 Current version: CORRECTED REFLC GEN:07.165 V8	DVD release (April 2004) ozoneaq.gsfc.nasa.gov/index.md * (September 2007)
OMIR AURA OMI	1.0×1.0	2004 2008	331	L3, JPM STD REFL340 GEN:06:089	toms.gsfc.nasa.gov/pub/omi/data/ (June 2010) toms.gsfc.nasa.gov/pub/omi/data/ (February 2010)
OMIR-hr AURA OMI	0.25×0.25	2004 2006	331	L3e, TO3 STD REFLECT, GEN:06:279	toms.gsfc.nasa.gov/omi-new/omi/data/Level3e/ (December 2009) toms.gsfc.nasa.gov/omi-new/omi/data/Level3e/ (September and October 2006)

* Please note that the reflectivity data is stored under “Radiative Cloud Fraction”.

performed for the UV wavelengths of interest using a full radiation transfer algorithm, while the impact of clouds enters by application of Cloud Modification Factors (CMFs). As a consequence of the integrations (daily sums and effective UV), CMFs are in principal dependent on the solar zenith angle and spectral weighting function or action spectrum but, fortunately, these dependencies are smooth and can be parameterized (Den Outer et al., 2005). For instance, important health topics currently under debate are UV-induced production of vitamin-D and its attributed beneficial effects versus the instances of skin cancer caused by UV radiation. The action spectra involved induce differences in absolute scale and in ozone sensitivity of the effective UV values, but are spectrally close enough so that the same cloud effect proxy suffices. Studies involving for instance UV-A exposure (wavelength of 315–400 nm), however, require a modification of the CMFs (Den Outer et al., 2005).

This paper is structured as follows. In Sect. 2, we present information on the data sources and restrictions we made and we discuss how we apply the reflectivity data to construct CMFs. In Sect. 3, an investigation is presented on the optimal area to be included in the CMF algorithm when applying reflectivity data to calculate the daily sums of UV radiation at the ground. An assessment of consistency and a search for improvements is then carried out in Sect. 4 by a comparison with CMFs derived from pyranometer measurements gathered at the World Radiation Data Centre. Pyranometers are chosen as they provide a much higher spatial density and are available for a much longer time period than ground-based UV irradiance measurements. The validity of the found improvements is tested through a comparison with ground-based UV irradiance measurements of eight European sites.

2 Used definitions and utilized data sets

In this paper the term “UV irradiance” denotes the erythemally weighted spectral irradiance at ground level integrated over wavelength (McKinley and Diffey, 1987). A daily UV sum will be the UV irradiance integrated over a day. Measured daily UV sums can be inferred from irradiance measurements delivered by spectroradiometers or broadband detectors, see Sect. 2.2. Spaceborne and modelled daily UV sums required application of a UV radiation transfer model with a cloud effect algorithm. We first calculate the clear sky daily UV sum and then the result is multiplied by a cloud modification factor (CMF) F to obtain the cloudy sky daily UV sum. Integration over time of previously calculated UV irradiances that are stored in a look-up table yields the clear sky UV sum. The look-up table has been calculated using the Tropospheric Ultraviolet and Visible Radiation Model, TUV (cprm.acd.ucar.edu/Models/TUV), and applies to a standard atmosphere. In this paper, the cloud modification factor F will always represent a factor to be applied to daily UV sums, and typically ranges from 0.1 to 1.1. If a CMF is inferred from ground-based measurements, e.g. Global Solar Irradiance (GSI) (Calbó et al., 2005) it will be denoted as F_{gb} . When spaceborne data is used, e.g. reflectivity (Eck et al., 1995; Herman and Celarier, 1997; Krotkov et al., 2001), we will write F_{sat} .

The spaceborne reflectivity data (Bhartia, 2002) basically returns the fraction of excess amount of radiation reflected by the atmosphere without the Rayleigh scattering contribution, and is measured in the UV-A range (see Table 1). The reflectivity r is expressed as a percentage and runs from what should be the ground albedo, a few percent, to 100%. Occasionally, values slightly over 100% are listed as well. For convenience, we apply a multiplication of 0.01 to all

r-values; F_{sat} is then essentially $1 - r$, c.f. Eck et al. (1995) who applied a binary ground albedo correction, and Herman et al. (2009) who give an expression of all multiple reflection between ground, clouds and scattering atmosphere.

In our approach, the reflectivity r is thought of as the result of all the multiple reflections in a cloud-ground system. All multiple reflections can be easily summed and the bare cloud reflection coefficient R_{cld} can be inferred:

$$r = (a + R_{\text{cld}} - 2aR_{\text{cld}}) / (1 - aR_{\text{cld}}) \quad (1a)$$

$$\rightarrow R_{\text{cld}} = (r - a) / (1 + ar - 2a), \quad (1b)$$

where a represents the ground albedo and sets the lower boundary for the reflectivity. Differences between reflections of “diffuse” and direct radiation have been omitted in Eq. (1a), and, only at this point, absorption is neglected. The total effect of clouds and ground albedo on the clear sky UV irradiance I_0 is then expressed as:

$$\begin{aligned} I &= I_0 \times F_{\text{sat}} = I_0 \times T_{\text{cld}} / (1 - aR_d) \\ &= I_0 \times (1 - R_{\text{cld}}) / (1 - aR_d), \end{aligned} \quad (2)$$

yielding the cloudy sky UV irradiance I . $T_{\text{cld}} = 1 - R_{\text{cld}}$ is the cloud transmission coefficient, and R_d is the combined effect of the cloud layer and the atmosphere, similar to Eq. (1a). The reflection by the cloud layer is assumed to be wavelength-independent. The downward reflection of upwelling radiation by the atmosphere is of course dependent on wavelength and is calculated using the UV radiation transfer model TUV. Equation (2) should be integrated over time to obtain the UV sums, and the second term of Eq. (2) becomes the sought cloud modification factor F_{sat} . It also includes the effect of the ground albedo that will be enhanced for solid overcast. Effects of surface elevation and aerosols enter predominantly in the clear sky irradiance I_0 , correction factors can then be applied or a different look-up table can be used. Aerosols and surface elevation also have a second order effect through their impact on R_d and Eq. (1). Absorbing aerosols reduce the effect of a high surface albedo for instance. Since Eq. (2) applies to wavelength-integrated quantities, R_d had to be integrated over wavelength as well; thereby it has become dependent on the considered action spectrum, solar zenith angle and ozone. For small albedos, the right hand side of Eq. (2) reduces to $1 - r$.

We will use ground-based ozone data and other available local ancillary measurements to calculate the so-called spaceborne UV sums or spaceborne UV irradiances; details of the used ancillary data can be found in Den Outer et al. (2010). This is because we want to evaluate only the cloud information of the satellite measurements. For the same reason, we do not incorporate in this study the erythemal UV products, also available on ozoneaq.gsfc.nasa.gov, because it tends to overestimate the actual erythemally weighted UV irradiance (Tanskanen et al., 2007).

2.1 Reflectivity

We utilize the reflectivity produced by N7-TOMS from 1979 to 1992, by EP-TOMS from 1996 to 2005, and by OMI from 2004 to 2008. Reflectivity produced by EP-TOMS is used until the year 2002, after 2002 calibration problems of this instrument emerge (Van Dijk et al., 2008; Herman et al., 2009). The available data produced by N7-TOMS and EP-TOMS is one data field per day on a latitude longitude grid of $1.0 \times 1.25^\circ$. As OMI has been adopted as the successor of EP-TOMS, its products have inherited the same format, although the delivered grid sizes have changed over time. First the format of the ozone and reflectivity data was on the same $1.0^\circ \times 1.25^\circ$ grid as the TOMS data, today it is delivered on a $1.0^\circ \times 1.0^\circ$ grid. Additionally, a high-resolution grid of $0.25^\circ \times 0.25^\circ$ is produced. Exclusively in Sect. 3, where we investigate the optimal grid size, we will make use of this high-resolution version of the OMI reflectivity data. The extensive comparison with ground-based measurements, Sect. 4, is carried out with OMI reflectivity data on a $1.0^\circ \times 1.0^\circ$ grid. We denote the reflectivity data set produced by N7-TOMS as “NIMBUS”, and EP-TOMS as “EP-TOMS”. The term “OMIR” indicates the reflectivity data set of OMI, and OMIR-hr the high resolution version. Details of used data sets and versions are given in Table 1. Only occasionally we will present results using the 2007 update of EPTOMS, “based on the NOAA-16 SBUV/2 ozone record.”

Overpass data for a long list of locations of meteorological stations is also produced and made available on the Ozone and Air Quality site (ozoneaq.gsfc.nasa.gov). Although differences exist between the gridded and overpass data versions, generally from our perspective, the use of either does not lead to different conclusions. Therefore, we do not present results using the overpass data sets and keep the number of different data sets and possible applied corrections to a surveyable level.

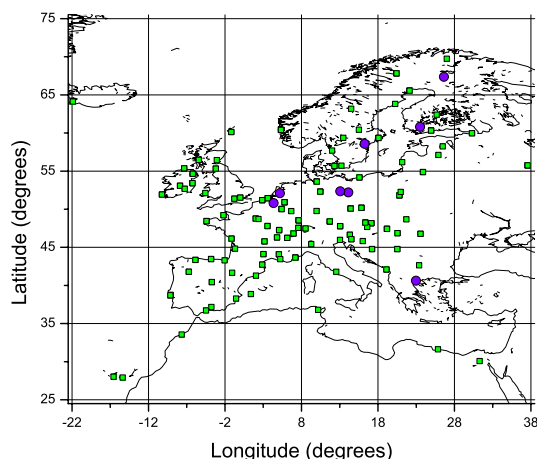
2.2 Ground-based UV irradiance

Daily sums of measured, erythemally weighted UV irradiances were delivered by each site operator of eight low-altitude UV radiation monitoring sites across Europe, see Fig. 1 and Table 2. The majority of these monitoring sites were selected in the SCOUT-O3 EC-project because of the availability of long-term quality controlled UV irradiance data. Data sets were re-evaluated in the context of the same project. Spectra are available at the European UV database, (<http://uv.fmi.fi/uvdb>) where, at submission, each spectrum undergoes an automatic quality flagging using the SHICrvm packages (Slaper et al., 1995) and the CheckUVspec package NILU, Norway (<http://zardoz.nilu.no/~olaeng/CheckUVSpec/CheckUVSpec.html>).

UV spectra are the basis of the produced daily UV sums for Bilthoven, Uccle, Jokioinen, Sodankylä, Potsdam and Lindenberg. For Thessaloniki, broadband data with a high

Table 2. UV radiation monitoring sites.

Site ID Place, Country	Lat. (°), Lon. (°) Height (m)	Instruments	Used data
FIS Sodankylä, Finland	67.36 26.63 179	Brewer MKII	04/1990–12/2006
FIJ Jokioinen, Finland	60.81, 23.49 107	Brewer MKIII	01/1996–12/2006
SEN Norrköping, Sweden	58.58, 16.15 43	RB SL501	03/1983–12/2008
DEP Potsdam, Germany	52.36, 13.08 107	Brewer MKII, MKIII	01/1995–04/2003
DEL Lindenberg, Germany	52.21, 14.12 127	Brewer MKIV, SPECTRO 320D	01/1996–12/2004 01/2005–12/2006
NLB Bilthoven, The Netherlands	52.12, 5.19 40	Broadband SL501 Dilor 2XY.50	02/1994–12/1995 02/1996–12/2008
BEU Uccle, Belgium	50.799, 4.357 100	Brewer MKIII UV-Biometer 501	01/2004–12/2008
GRT Thessaloniki, Greece	40.63, 22.95 60	Broadband YES UVB-1 erythemal detector	08/1991–12/2006

**Fig. 1.** Locations of WRDC stations (green squares) and UV monitoring stations (violet circles) in Europe, all UV monitoring stations are WRDC stations as well. Grid lines indicate the super grid cells used to determine underlying correlations.

temporal resolution (one measurement per minute) is used. The broadband data is calibrated against two collocated Brewer spectroradiometers. The Norrköping UV data set is fully broadband-based; this data series was previously extensively re-evaluated, and relative spectral correction functions were applied. The main characteristics of each monitoring site and references to operation protocols can be found in Den Outer et al. (2010). The measurement regime for all sites

is from sunrise to sunset, with some variations in choice of tolerance.

The period prior to the onset of ground-based UV radiation monitoring is covered by modelled UV sums. The modelled UV sums are taken from the so-called best estimate derived in Den Outer et al. (2010). In this paper, series of daily UV sums derived from ground-based UV irradiance measurements and from five different UV reconstruction models were intercompared and an iterative procedure was set up that delivered one best estimate of the historical daily UV sums at ground level. The procedure takes into account the long-term stability and underlying agreement of the models, and the agreement with actual UV irradiance measurements for the period with UV measurements. It delivers a recalibration factor and a statistical weight for each modelled and measured series. The modelled series are rescaled such that the recalibration factor for the measured series becomes 1. Depending on the availability of model input data, the best estimates start well before the pre-satellite period for most sites, i.e. the mid-sixties. The UV reconstruction models used ground-based measured data like total column ozone, GSI, aerosol climatology, snow depth, etc. A minimum requirement was the availability of measured total column ozone and GSI. The best estimates are used for the entire period covered by NIMBUS, for Thessaloniki until 1980, Norrköping until 1984, and for Uccle until 2004.

Data gaps occurring in the measured UV series after the onset of the UV radiation monitoring will not be supplemented with ground-based modelled data. Even so, data gaps in the best estimates (unavailable ozone or GSI data) will not

be supplemented either. With respect to irradiance levels and distributions of daily UV sums, the residual differences between the best estimates and actual measurements are small, and much smaller than can be expected from a comparison of spaceborne versus ground-based observations. Therefore, in the rest of the paper we will use “measured” UV to indicate both origins of the ground-based UV sums.

2.3 Ground-based global solar irradiance

The World Radiation Data Centre (WRDC) located in St. Petersburg, Russia, holds valuable data records of historical GSI-measurements (wavelength range 300–3000 nm) dating from the year 1964, when the data centre was founded. During a COST-726 action project (www.cost726.org), and in close collaboration with the WRDC staff, the daily sums of GSI for the European continent were extracted, quality checked and brought to the standard World Radiometric Reference scale if not already applied. The data set was made available within the community of the COST-project. We make use of this data set and have selected over 83 locations with sufficient data in the European continent. By “sufficient” we mean a data record covering more than three years, with over 50 % of the days per year available. Additional data for the period after 2004 and for a few African stations was extracted through direct access to the WRDC database. Only stations situated at altitudes below 750 m were chosen. The GSI data is transformed to cloud modification factors by applying the algorithm described in Den Outer et al. (2005), and indicated as F_{gb} in the rest of this paper. This algorithm is an empirically established relationship between measured and ground-based modelled daily UV sums. The relationship is dependent on classes of solar zenith angles and applied wavelength regimes.

3 Optimal area

The agreement between any satellite-derived quantity and its ground-based measured counterpart will, among underlying intrinsic agreements, also be a function of the areas that are effectively intercompared. In our case, we expect an optimal agreement when the satellite measurements used to calculate F_{sat} are derived for an area, $A_{F_{sat}}$, that is representative for the clouds drifting over the ground station during “midday”. The sky properties at midday dominate because of the high solar elevation angle which delivers the largest portion of the total daily UV sum. An $A_{F_{sat}}$ that is too small will likely sample a non-representative fraction of the actual cloud layer. An $A_{F_{sat}}$ that is too large disregards the extremes due to the averaging in the first place and secondly, it incorporates clouds that in reality do not influence the UV irradiance at the particular ground station because of their location and wind direction/speed or may have dissolved at the time

of arrival at the overhead location of the ground station. Similarly, the reverse applies for cloudless spots within $A_{F_{sat}}$.

Note that the agreement with a UV irradiance measurement at the time of overpass will not improve automatically when a small $A_{F_{sat}}$ is used. UV irradiance measurements have a large contribution of scattered radiation, even on cloudless days it is around 50 %, and a large area surrounding the site, 10 to 30 km, is of influence. The presence of clouds in the whole hemisphere is of importance and not only the clouds at zenith or in the direction of the sun. An $A_{F_{sat}}$ that is too small would lead to erroneously assigning only the overhead clouds to be of influence.

We vary the size of $A_{F_{sat}}$ to investigate the existence of an optimum for application of reflectivity data in a cloud effect algorithm for daily UV sums. The starting point is the reflectivity of the high-resolution ($0.25^\circ \times 0.25^\circ$) OMI grid cell overhead the ground station. Next, we gradually increase the number of considered $0.25^\circ \times 0.25^\circ$ -grid cells adjacent to the overhead grid cell, thereby increasing $A_{F_{sat}}$ accordingly. We compare the accompanying UV sum with those measured at the ground stations. The results are shown in Fig. 2. The number of grid cells in longitudinal direction is approximately $1/\cos(\text{latitude})$ times the number of grid cells in latitudinal direction to perform the analysis on square areas. The ozone values are not varied and are taken from the ground-based observations. We also show the results using OMIR data for the same days as contained in the OMIR-hr data. The area of $A_{F_{sat}}$ is indicated by the size in degrees in the latitudinal direction.

An optimum occurs for $A_{F_{sat}}$ of approximately 1.0 to 1.5° , where the averaged ratios of model to measured daily UV sums have minimum standard deviations. The increase of the standard deviations towards larger $A_{F_{sat}}$ turns out to be independent of location of the ground-based stations. The Lindenberg data behaves a bit differently in this respect. The averaged level of the ratios may vary with the size of $A_{F_{sat}}$. Six sites show an increase, while data of Lindenberg and Thessaloniki show a decrease with an increasing $A_{F_{sat}}$. The averaged reflectivity for all WRDC sites together turns out to be independent of the number of averaged adjacent grid cells, i.e. the size of $A_{F_{sat}}$. Hence, the observation that the averaged level of the ratios vary, can be regarded as an artefact due to the subset of these eight sites.

An optimal $A_{F_{sat}}$ of 1.5° is quite a reasonable number because 1.5° corresponds to an area (170×170 km for the Netherlands) that can be easily traversed by clouds during a few hours. We calculated the averaged wind speed of one year (2010) using the HIRLAM-6 meteorological fields at 1350 m a.s.l. (above sea level) (HIRLAM, 2012). The direction of the wind was disregarded in this calculation. Generally, the averaged speeds are higher above the sea west of Great Britain, i.e. $10\text{--}12 \text{ m s}^{-1}$, than above land, i.e. $6\text{--}10 \text{ m s}^{-1}$. For the eight locations of the UV radiation monitoring sites, the yearly averaged wind speeds range from 6.7 to 9.7 m s^{-1} ; the smallest values were found in Finland

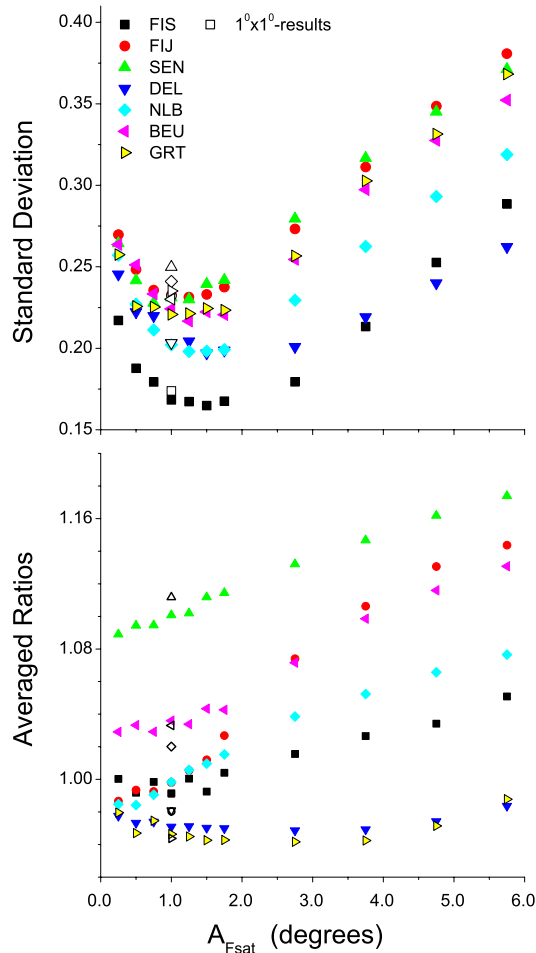


Fig. 2. Standard deviations (top panel) and averages (bottom panel) are plotted for ratios of spaceborne to measured daily UV sums for the OMI-period as a function of the area included in the spaceborne algorithm, $A_{F_{\text{sat}}}$. The area $A_{F_{\text{sat}}}$ is square-shaped, its size indicated in the latitudinal direction and overhead each monitoring site. Symbols and colours code to the UV monitoring site indicated by the legend (top panel), the key to monitoring sites is listed in Table 2. The results using the $1^\circ \times 1^\circ$ -grid cells are shown as open symbols; concurrent days per site with respect to the OMIR and OMIR-hr data sets are used.

and the highest in Bilthoven, Lindenberg and Potsdam. This means that clouds drift in about 5 to 7 h through the area set by the optimum $A_{F_{\text{sat}}}$. Since the measurement of the reflectivity is close to local noon, it captures the clouds that contribute mostly to the reduction of the daily UV sum. Seven hours centred at noon captures approximately 80 and 95 % of the daily UV sum in The Netherlands for the summer and winter half year, respectively.

The HIRLAM fields at 1350 m were chosen because 1350 m is right in the middle of the distribution of the cloud base height measured at Cabauw, a meteorological site near Bilthoven. The distribution of the cloud base height is broad, almost flat up to 2 km (75 % is below 2000 m) and tails off

Table 3. The slopes of a linear fit to the ratios $F_{\text{sat}}/F_{\text{gb}}$ (a logarithmic scale) as function of time, and averages of $F_{\text{sat}}/F_{\text{gb}}$ using data from all WRDC ground stations. The uncorrected results (Uncor) are listed as well as the results corrected to the one-to-one line (Cor211) and to the curve found for the EPTOMS SZA1-interval (Cor2A1).

Data set	slope [10^{-3} yr]	$\langle F_{\text{sat}}/F_{\text{gb}} \rangle$		
		Uncor.	Cor211	Cor2A1
NIMBUS	$+3.8 \pm 0.1$	0.92 ± 0.30	0.99 ± 0.33	0.94 ± 0.31
EPTOMS*	-1.9 ± 0.5 $+6.7 \pm 0.5$	0.91 ± 0.27 0.98 ± 0.76	0.99 ± 0.29 –	0.93 ± 0.28 –
OMIR	28 ± 1	0.86 ± 0.35	1.00 ± 0.40	0.95 ± 0.38

* Figures on the second line apply to the EPTOMS update 2007.

to 10000 m. We conclude that the current grid sizes of the reflectivity data ($1.0^\circ \times 1.0^\circ$ and $1.0^\circ \times 1.25^\circ$) are a good, or even optimal, choice for calculating the cloud effect for daily UV sums.

4 Comparison

4.1 Spaceborne versus ground-based cloud modification factors

The ground-based CMFs, F_{gb} , are calculated from the GSI data of all eighty WRDC stations; the corresponding spaceborne CMFs, F_{sat} , were calculated using the data sets NIMBUS, EPTOMS, and OMIR. We obtained 380 k (86 %), 140 k (75 %), 80 k (83 %) pairs of CMFs (spaceborne, ground-based) for the NIMBUS, EPTOMS and OMIR, respectively. Percentages indicate fractions with respect to the maximum number of pairs considering the time period and number of WRDC-stations.

We first tested the long-term stability by making linear fits to the ratios $F_{\text{sat}}/F_{\text{gb}}$ plotted as a function of time (see Table 3). The found slopes are indeed small, except for the OMIR. Here the considered period is a bit too short to make the linear fits. Bilthoven has one year extra, and using these data only we found no significant slope ($5.6 \pm 5.5) \times 10^{-3} \text{ yr}^{-1}$. We tested the 2007 update of EPTOMS in the same manner. We see a change of sign and a somewhat greater linear coefficient (from $-1.9 \times 10^{-3} \text{ yr}^{-1}$ to $+6.7 \times 10^{-3} \text{ yr}^{-1}$) compared to the 2004 version. The standard deviation, listed also in Table 3, has increased. This is mainly due to the larger scatter of the ratios in winter time (range 0.14–100), which is absent for the EPTOMS of 2004 (range 0.17–9). Therefore, our principal data set for EPTOMS will be the data obtained in 2004.

Next we made plots of F_{gb} versus F_{sat} and show the results as density of data points in Fig. 3. In fact, we have plotted F_{gb} versus $1 - r$ thereby neglecting the enhancement of the irradiance due to ground albedo. Since all CMFs

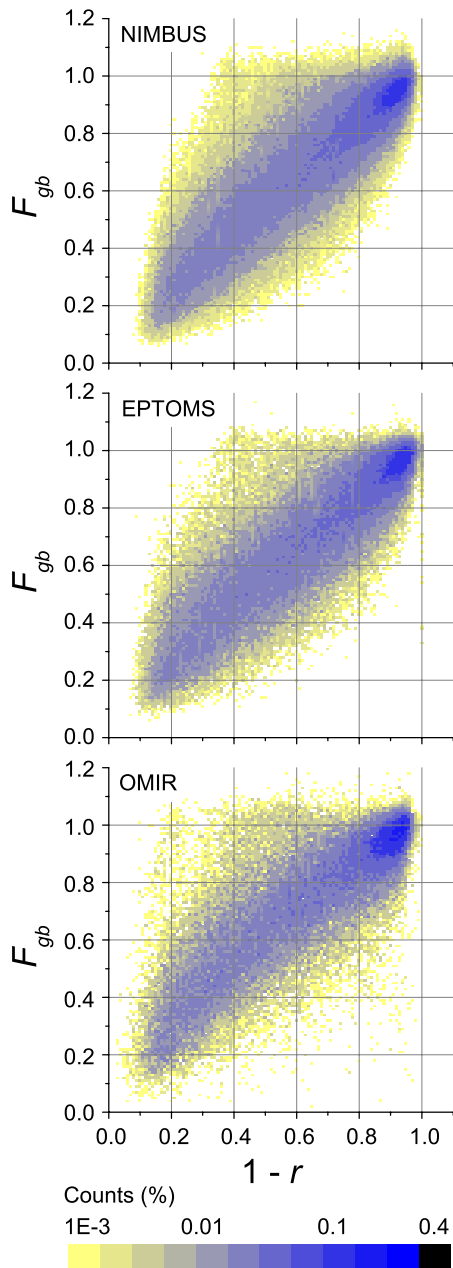


Fig. 3. Density plots of cloud modification factors (CMF), F_{gb} , paired with co-located satellite-based reflectivity r measurements for the data sets indicated. Year-round data is shown; corrections for ground reflections (ground albedo) have not been applied.

apply to the UV wavelength range, we expect to observe linear relationships, i.e. the highest density along the line with slope 1 through the origin. The difference between the data measured by OMI and the two TOMS instruments is striking. A linear relationship is indeed revealed in the EPTOMS and NIMBUS plots, while the plot of the OMIR-based CMFs has a convex shape. The distributions of the r -values, shown in Fig. 4, also hint at a different behaviour of

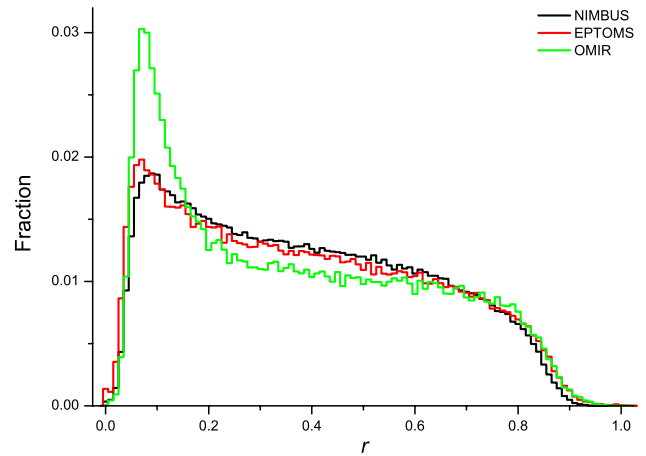


Fig. 4. The distributions of reflectivity r for the data sets indicated are plotted.

OMIR versus EPTOMS and NIMBUS. All reflectivity distributions peak at a reflection of 0.08 and have an average value of 0.37 for the three instruments. However, the OMIR distribution peaks much higher than the distributions found for EPTOMS and NIMBUS. The grid size of the final products, OMIR a little smaller than that of EPTOMS and NIMBUS, i.e. $1.0^\circ \times 1.0^\circ$ versus $1.0^\circ \times 1.25^\circ$, cannot explain this observation. Roughly the same distribution is found for OMIR, meaning a severe reduction of the dynamic range is not observed when we apply a 4-point grid cell average (distant-weighted) prior to the calculation of the distribution. A thorough explanation is a bit beyond the scope of our paper but several mechanisms and distinct differences between the three instruments may cause the different distributions. The spatial resolution of the orbital scans corresponds to a surface area of approximately $50 \text{ km} \times 50 \text{ km}$, $39 \text{ km} \times 39 \text{ km}$, and $13 \text{ km} \times 24 \text{ km}$ for N7-TOMS, EP-TOMS, and OMI, respectively. The grid cells correspond to areas of about $110 \text{ km} \times 70 \text{ km}$ (or $110 \text{ km} \times 86 \text{ km}$ for the $1.0^\circ \times 1.25^\circ$ grid) in Western Europe. Since there are more overpasses by OMI than N7-TOMS and EP-TOMS, the number of grid cells from truly nadir-viewed pixels will also be greater for OMI. Due to the three-dimensional extension of clouds, non-nadir viewing directions will then lead to more cloudy assigned pixels. The variability of the OMI pixels might therefore be much higher than that of EP-TOMS and N7-TOMS. The higher variability is preserved during the construction of the grid cell values, despite the larger number of pixels needed for OMIR. In line with this reasoning, the EPTOMS distribution is slightly more peaked than the distribution of NIMBUS.

The idea now is to educe a single curve that characterises the correlation in the scatter of data points as it comes forward in each data set of Fig. 3, and determine an empirical relationship that can be applied to improve the satellite-derived CMFs. The curve formed by the connected local maxima, in

analogy to a mountain ridge if the density was plotted on the z-axis, can be used best to pin the correlation between spaceborne CMFs and ground-based CMFs. The locations of the local maxima are sought by moving an imaginary line with slope -1 over the density plot of Fig. 3 and recording the locations of the maxima along this line while moving. A line with slope of -1 is roughly perpendicular to the orientation of the so-called ridge. Other slopes, except 1, lead to similar locations of the local maxima in the density plots. This procedure automatically disregards CMF pairs obtained on days with snow cover, i.e. high-ground albedo, as these data points show up as outliers. We tested the variations in the correlation among subsets of the data: i.e. grouping with respect to location, latitude, and SZA intervals. SZA denotes the minimal Solar Zenith Angle reached for the day and location of the considered data point. We made the density plots for latitude bands and for $10^\circ \times 10^\circ$ grid cells shown in Fig. 1. Only a dependency could be determined on the SZA for the shape (of the ridges) of these density plots. Thus for the European continent, it is sufficient to group data only with respect to the SZA. Trial and error lead to a most efficient set of SZA-intervals as given in Fig. 5. The first two SZA-intervals deliver the same curve using NIMBUS and EPTOMS, and although the shape is close to the ideal one-to-one relationship, small improvements can be established. The shape of the ridges for the higher SZA boundaries deviates clearly from a straight line. Ridges produced using OMIR are even more curved.

We fitted 4th-order polynomials to the ridges and use these fit functions to correct r-values. In this way, we correct the satellite-derived CMF such that it will yield, on average, the ground-based CMF constructed from GSI. Using 4th-order terms is rather overdimensionalized but here we only want to establish a numerical expression for the found data ridges and do not develop a theory that would explain the mechanism behind these correlations. Our ultimate goal is to improve on the spaceborne UV sums. For this reason, we do not list the determined eighty coefficients (4 instruments times 4 SZA intervals times 5 fit parameters), but they are available on request.

Triggered by previous results (Matthijssen et al., 2000; Williams et al., 2004), which essentially state that the bare implementation of EPTOMS should lead to good results, we have set up an alternative correction scheme. Instead of correcting to the ideal one-to-one line, the EPTOMS-ridge obtained for the smallest SZA-interval is deemed the ideal curve describing the correlation between F_{gb} versus F_{sat} (the black curve EPTOMS panel of Fig. 5). Thus, we make all the other ridges EPTOMS-like. Correcting to the corresponding NIMBUS curve would have led to the same results for that matter.

We test three ways of correcting the delivered r-values before these values enter the CMF-calculation:

1. uncorrected implementation

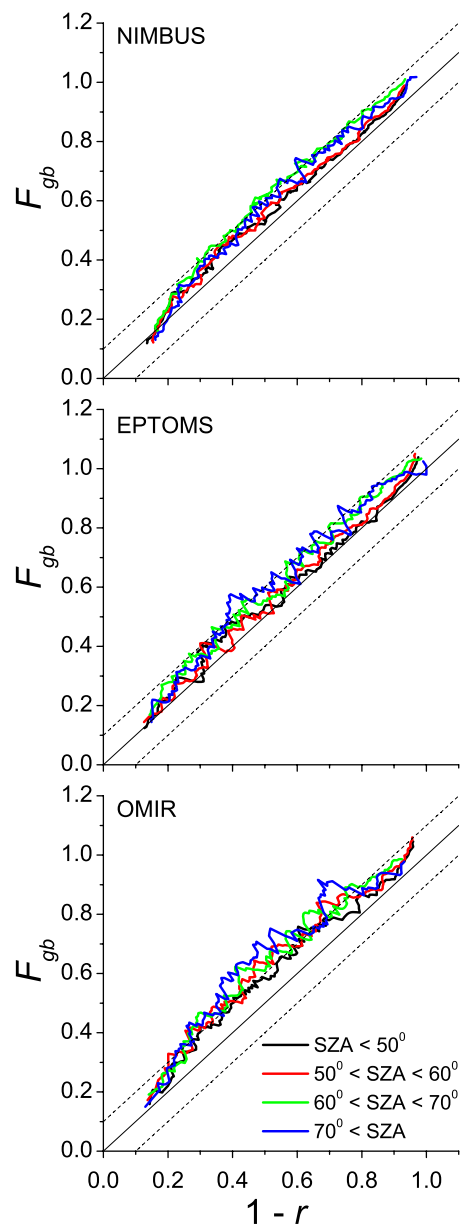


Fig. 5. The ridges of the density plots in Fig. 3 are shown. Data is grouped per SZA-interval as indicated in the bottom panel, and is the same for all. Additional shifted $x = y$ grid lines are plotted to emphasize the observed differences between NIMBUS and EPTOMS as well as OMIR.

2. corrected to the one-to-one line
3. corrected to the curve found for the EPTOMS SZA1-interval.

The three implementations will be indicated by Uncor, Cor211 and Cor2A1 for the implementations 1, 2 and 3, respectively.

In Table 3, the result for the CMFs is summarized by the average of satellite- versus ground-based derived CMFs. The

Table 4. The averages of the ratios spaceborne to ground-based measured daily UV sums are listed for days where $F_{gb} < 0.2$ (all sites together). The logarithmic averaging was applied, the standard deviation then translates to the range indicated between brackets. The dependency of these ratios on F_{gb} for $F_{gb} > 0.2$ is expressed as a value of the linear coefficient of a linear fit (fourth column). Uncorrected results (Uncor), results corrected to the one-to-one line (Cor211) and to the curve found for the EPTOMS SZA1-interval (Cor2A1) are listed.

Data set	Correction	Averages	Linear term $0.2 < F_{gb} < 1.2$
NIMBUS	Uncor	1.04 (0.72–1.49)	-0.009 ± 0.002
	Cor211	1.18 (0.80–1.72)	-0.069 ± 0.002
	Cor21	1.05 (0.71–1.55)	-0.021 ± 0.002
EPTOMS	Uncor*	1.00 (0.68–1.49)	0.029 ± 0.004
		1.11 (0.76–1.62)	0.000 ± 0.004
	Cor211	1.22 (0.85–1.76)	-0.038 ± 0.003
	Cor2A1	1.05 (0.71–1.56)	0.018 ± 0.004
OMIR	Uncor	0.87 (0.61–1.23)	0.092 ± 0.007
	Cor211	1.18 (0.83–1.68)	-0.047 ± 0.006
	Cor2A1	1.04 (0.73–1.49)	0.012 ± 0.007

* Figures on the second line apply to the EPTOMS update 2007.

average is calculated using the data from all WRDC ground stations. Obviously, the Cor211 leads to an average close to one, and the Cor2A1 leads to smaller values. The uncorrected OMIR produces a 7% smaller value for the average F_{sat} compared to uncorrected NIMBUS and EPTOMS: 0.86, compared to 0.92 and 0.91 respectively.

4.2 Spaceborne versus ground-based UV sums

In Fig. 6, the effect in the UV wavelength range of the three implementations is shown by plotting the ratios of spaceborne to measured daily UV sums as a function of F_{gb} ; the ideal algorithm should then be independent of this variable. A general algorithm to cope with high-ground albedos is applied, using ancillary data on snow cover supplied by the site operators. A different SZA-interval is chosen in each panel for presentation reasons, where it should be mentioned that intervals for the smaller SZAs, if applicable, show better results, i.e. smaller scatter and closer to 1. The uncorrected implementation, shown in the insets of Fig. 6, generally leads to ratios smaller than 1 in all cases, as follows also from the shape and location of the curves in Fig. 5. Table 4 put numbers to the behaviour as seen in Fig. 6. We list the average values of the ratios for $F_{gb} < 0.2$, and give the slope of linear fits to these ratios for the part $F_{gb} > 0.2$. In both cases, we first took the logarithm of the ratios to put an even statistical weight on ratios larger or smaller than 1. Implementation of Cor211 apparently leads to overestimation of the daily UV sums, especially at solid overcast. The best results were obtained with the Cor2A1-implementation, by which

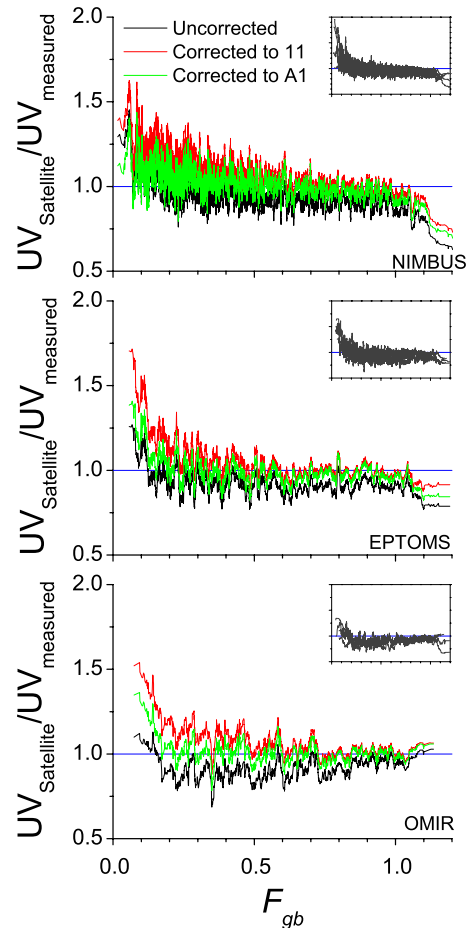


Fig. 6. Ratios of daily sums are plot as function of the ground-based CMF, 31-points running means are shown only. A different SZA-interval is chosen for presentation reasons in each panel. The SZA-interval are NIMBUS: $70^\circ < \text{SZA}$, EPTOMS: $60^\circ < \text{SZA} < 70^\circ$, OMIR: $50^\circ < \text{SZA} < 60^\circ$. Insets show 31-point running mean uncorrected averages for all SZA-intervals.

we obtain the smallest absolute slopes and averages. The EPTOMS 2007 update shows a better slope for the linear fit, but the average for $F_{gb} < 0.2$ increased.

In Table 5, we list the averaged ratios of spaceborne to ground-based measured daily UV sums for the three implementations. Slightly improved overall results are indeed obtained for NIMBUS and EPTOMS, as shown by the “Cor2A1”-columns. The more northern sites have benefited most from the applied corrections. The results using OMIR have undergone improvements of 10%. The day-to-day variability, reflected in the listed standard deviations is insensitive to the applied correction. The slopes and the average of the uncorrected implementations set OMIR apart from NIMBUS and EPTOMS.

Clouds above a high-ground albedo, i.e. snow cover, leads to multiple passes of the radiation through the boundary layer, which, in turn, could lead to enhanced absorption of

Table 5. Averaged ratios of spaceborne to ground-based measured daily UV sums. For the three reflectivity data sets NIMBUS, EPTOMS and OMIR. Uncorrected (Uncor) results, corrected to the one-to-one line (Cor211) and to the curve found for the EPTOMS SZA1-interval (Cor2A1) are listed. Last row: results for all sites together, key to monitoring sites in Table 2.

	Lat. (°)	NIMBUS			EPTOMS			OMIR		
		Uncor	Cor211	Cor2A1	Uncor	Cor211	Cor2A1	Uncor	Cor211	Cor2A1
FIS	67.37	0.94 ± 0.22	1.04 ± 0.24	0.97 ± 0.23	0.95 ± 0.22	1.06 ± 0.23	0.98 ± 0.23	0.86 ± 0.16	1.05 ± 0.18	0.99 ± 0.17
FIJ	60.82	0.96 ± 0.22	1.06 ± 0.25	1.00 ± 0.24	0.95 ± 0.26	1.03 ± 0.28	0.97 ± 0.27	0.83 ± 0.24	1.01 ± 0.27	0.95 ± 0.26
SEN	58.58	1.06 ± 0.30	1.16 ± 0.35	1.09 ± 0.32	0.98 ± 0.25	1.07 ± 0.29	1.02 ± 0.27	0.98 ± 0.27	1.18 ± 0.35	1.12 ± 0.32
DEP	52.36	0.95 ± 0.25	1.03 ± 0.28	0.97 ± 0.26	0.95 ± 0.27	1.04 ± 0.30	0.98 ± 0.28			
DEL	52.21	0.93 ± 0.25	1.00 ± 0.27	0.95 ± 0.26	0.88 ± 0.23	0.96 ± 0.25	0.90 ± 0.24	0.86 ± 0.24	1.02 ± 0.26	0.97 ± 0.26
NLB	52.12	1.00 ± 0.27	1.08 ± 0.29	1.02 ± 0.28	1.02 ± 0.33	1.11 ± 0.36	1.05 ± 0.34	0.93 ± 0.23	1.10 ± 0.27	1.04 ± 0.26
BEU	50.80	0.99 ± 0.24	1.07 ± 0.26	1.01 ± 0.24	0.96 ± 0.25	1.05 ± 0.26	0.99 ± 0.25	0.93 ± 0.26	1.11 ± 0.29	1.04 ± 0.28
GRT	40.63	0.97 ± 0.26	1.02 ± 0.27	0.98 ± 0.26	0.98 ± 0.22	1.03 ± 0.24	0.99 ± 0.22	0.90 ± 0.22	1.01 ± 0.25	0.97 ± 0.24
ALL	–	0.98 ± 0.25	1.06 ± 0.28	1.00 ± 0.26	0.96 ± 0.25	1.05 ± 0.28	0.99 ± 0.26	0.90 ± 0.23	1.06 ± 0.27	1.01 ± 0.25

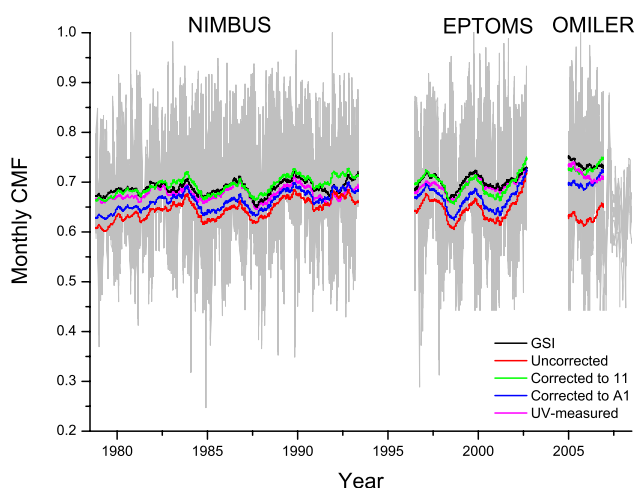


Fig. 7. Monthly CMFs for all sites, grey. Running means are shown in colour as indicated by the legend. We calculated the running means until 2007, because afterwards, data is limited to 3 sites.

UV radiation in the presence of tropospheric ozone. Since overestimations at solid overcast, as seen in Fig. 6, do not emerge that dramatically when using CMFs based on GSI, enhanced absorption by tropospheric ozone is likely not to play an important role. Thus the observed overestimations should be treated as limitations of the algorithm.

Table 6 lists the averaged ratios of spaceborne to measured monthly and yearly UV sum for all eight sites together. Values using F_{gb} are given as well. Again, similar observations can be made for the performance of NIMBUS and EPTOMS on the one hand, and OMIR on the other, where the latter has undergone a true improvement. Of course, for the winter half year NIMBUS and EPTOMS also yield monthly UV sums (October–February) that are too small. This is the reflection of SZAs being large during winter and that only for large SZAs deviating correlations were found (cf. Figs. 3 and 5). Yearly UV sums – with relatively small contributions from the winter half year – show only for OMIR an

actual improvement of the averaged ratios. The standard deviations in the F_{sat} -derived monthly UV sums are larger than using F_{gb} , while for the yearly UV sums this again just holds for the OMIR results.

In Fig. 7, we illustrate the effect of the performed analysis on long-range timescales. The CMFs for monthly sums, i.e. the cloudy sky monthly UV sums divided by the cloudless sky monthly UV sums, have been calculated for all sites and are plotted simultaneously in this figure. The shown running means are based on averaging a number of monthly CMFs determined by the available number of monthly UV sums per year times the number of sites. Here the necessity to apply corrections is again brought to the fore. While the uncorrected reflectivity-based F_{sat} do not follow the general trend inferred from the UV measurements, mainly due to OMIR, and would have indicated a downward trend, the corrected values follow the measured observation more closely and indicate an upward trend of the UV irradiance. The latter is in line with findings presented by Douglass and Fioletov (2011).

5 Conclusions

We have analysed the performance of the reflectivity data of three consecutive spaceborne instruments when applied in algorithms to determine ground-level ultraviolet irradiances. We made a comparison with CMFs derived from ground-based global solar radiation measurements from over eighty WRDC-stations and with UV irradiances measured at eight monitoring sites in Europe. Both comparisons lead to the observation that firstly, reflectivity data can be used as cloud effect proxy for UV irradiances at ground level. Secondly, the reflectivity data sets delivered by the TOMS on Nimbus 7 and TOMS on Earth Probe require only small corrections and for large SZAs only, and thirdly, corrections are substantial for OMIR where a 10 % underestimation in the derived daily UV sums is found for the uncorrected data. The long-term analysis shows that uncorrected reflectivity data could then lead

Table 6. Averaged ratios of spaceborne to ground-based measured monthly and yearly UV sums, all eight sites together. Monthly sums are listed separately for the summer (April–September) and winter months (October–March). Uncorrected (Uncor) results, corrected to the one-to-one line (Cor211) and to the curve found for the EPTOMS SZA1-interval (Cor2A1) are listed. Results using pyranometer data (GSI) to calculate F are shown as well.

UV sums		Data set			
		F based on	NIMBUS	EPTOMS	OMIR
Monthly	Summer	Uncor	0.98 ± 0.06	0.98 ± 0.07	0.94 ± 0.05
		Cor211	1.03 ± 0.06	1.02 ± 0.07	1.04 ± 0.06
		Cor2A1	0.98 ± 0.06	0.98 ± 0.07	1.01 ± 0.05
		GSI	1.02 ± 0.04	1.02 ± 0.05	1.04 ± 0.04
	Winter	Uncor	0.93 ± 0.12	0.89 ± 0.12	0.87 ± 0.16
		Cor211	1.03 ± 0.13	1.00 ± 0.12	1.05 ± 0.17
		Cor2A1	0.98 ± 0.13	0.95 ± 0.12	1.00 ± 0.17
		GSI	1.01 ± 0.12	1.01 ± 0.08	1.06 ± 0.11
Yearly	Uncor	0.98 ± 0.03	0.97 ± 0.04	0.93 ± 0.04	
	Cor211	1.03 ± 0.03	1.02 ± 0.04	1.04 ± 0.04	
	Cor2A1	0.98 ± 0.03	0.98 ± 0.04	1.00 ± 0.04	
	GSI	1.01 ± 0.03	1.01 ± 0.03	1.04 ± 0.03	

to a conclusion of a decrease of the UV irradiance in Europe, while the corrected version leads to the opposite. The latter is in line with findings based on pyranometer measurements and on UV irradiance measurements. This also shows that a long-term comparison of ground-based and satellite-based observations derived from different instruments is relevant in view of data continuity and homogeneity.

The overall best results were obtained unexpectedly with the correction that utilizes the initial correlation function between reflectivity of the TOMS instrument of Earth Probe and ground-based cloud modification factors, i.e. the Cor2A1 implementation, and not the Cor211 implementation. The current calibration of the reflectivity algorithm applied to OMI measurements produces deviating results compared to those produced by TOMS on Nimbus 7 and TOMS on Earth Probe and the former calibration of OMI measurements that have been used to produce the high-resolution reflectivity data set. The reflectivity data sets of the TOMS instruments have quite a consistent performance with respect to the CMFs derived using the WRDC data set. This justifies the use of EPTOMS until the year 2002 for CMF-calculations and, hence, long-term trend analysis.

The optimal area used for daily UV sum calculations is 1.0 to 1.5° in latitudinal direction for the European continent; smaller or greater sizes lead to higher standard deviations in the comparison of satellite versus ground-based daily UV sums. This area is roughly comparable with the distances that clouds traverse within 5 to 7 h over land.

Acknowledgements. Part of this work has been performed as part of the European Commission funded project SCOUT-O3 contract 505390-GOCE-CT-2004 and by the European Cooperation in Science and Technology (COST)-726. The work of RIVM was supported by the Strategic Research Projects COURSE and Di-light & Food. The work of A. V. Lindfors was funded by the Academy of Finland, decision 133259. We wish to acknowledge M. Brinkenbergh from the Cabauw Experimental Site for Atmospheric Research, The Netherlands for the use of the cloud height measurements.

Edited by: P. Stammes and P. K. Bhartia

References

- Arola, A., Kazadzis, S., Lindfors, A., Krotkov, N., Kujanpää, J., Tamminen, J., Bais, A., di Sarra, A., Villaplana, J. M., Brogniez, C., Siani, A. M., Janouch, M., Weihs, P., Webb, A., Koskela, T., Kouremeti, N., Meloni, D., Buchard, V., Auriol, F., Ialongo, I., Staneck, M., Simic, S., Smedley, A., and Kinne, S.: A new approach to correct for absorbing aerosols in OMI UV, *Geophys. Res. Lett.*, 36, L22805, doi:10.1029/2009GL041137, 2009.
- Barnes, R. A., Eplee, R. E., Schmidt, G. M., Patt, F. S., and McClain, C. R.: Calibration of SeaWiFS, I. Direct Techniques, *Appl. Optics*, 40, 6682–6700, 2001.
- Bhartia, P. K.: OMI Algorithm Theoretical Basis Document Volume II OMI Ozone Products, http://eosps.gsfc.nasa.gov/eos_homepage/for_scientists/atbd/docs/OMI/ATBD-OMI-02.pdf (last access: 6 December 2012), 2002.
- Bovensmann, H., Burrows, J. P., Buchwitz, M., Frerick, J., Noël, S., Rozanov, V. V., Chance, K. V., and Goede, A. P. H.: SCIAMACHY: Mission Objectives and Measurement Modes, *J. Atmos. Sci.*, 56, 127–150, doi:10.1175/1520-0469(1999)056<0127:SMOAMM>2.0.CO;2, 1999.

- Burrows, J. P., Weber, M., Buchwitz, M., Rozanov, V., Ladstätter-Weissenmayer, A., Richter, A., DeBeek, R., Hoogen, R., Bramstedt, K., Eichmann, K.-U., Eisinger, M., and Perner, D.: The Global Ozone Monitoring Experiment (GOME): mission concept and first scientific results, *J. Atmos. Sci.*, 56, 151–175, doi:10.1175/1520-0469(1999)056<0151:TGOMEG>2.0.CO;2, 1999.
- Calbó, J., Pagès, D., and Gonzalez, J.-A.: Empirical studies of cloud effects on UV radiation: A review, *Rev. Geophys.*, 43, RG2002, doi:10.1029/2004RG000155, 2005.
- Den Outer, P. N., Slaper, H., and Tax, R. B.: UV radiation in the Netherlands: Assessing long-term variability and trends in relation to ozone and clouds, *J. Geophys. Res.*, 110, D02203, doi:10.1029/2004JD004824, 2005.
- Den Outer, P. N., Slaper, H., Kaurola, J., Lindfors, A., Kazantzidis, A., Bais, A. F., Feister, U., Junk, J., Janouch, M., and Josefsson W.: Reconstructing of erythemal ultraviolet radiation levels in Europe for the past 4 decades, *J. Geophys. Res.*, 115, D10102, doi:10.1029/2009JD012827, 2010.
- Douglass, A. and Fioletov, V. (coordinating Lead Authors): Stratospheric Ozone and Surface Ultraviolet Radiation, in: Chapter 2 in Scientific Assessment of Ozone Depletion: 2010, Global Ozone Research and Monitoring Project-Report No. 52, World Meteorological Organization, Geneva, Switzerland, 516 pp., 2011.
- Eck, T. F., Bhartia, P. K., and Kerr J. B.: Satellite estimation of spectral UVB irradiance using TOMS derived total ozone and UV reflectivity, *Geophys. Res. Lett.*, 22, 611–614, doi:10.1029/95GL00111, 1995.
- Eskes, H., van Velthoven, P., Valks, P., and Kelder, H.: Assimilation of GOME total ozone satellite observations in a three-dimensional tracer transport model, *Q. J. Roy. Meteorol. Soc.* 129, 1663–1681 doi:10.1256/qj.02.14, 2003.
- Herman, J. R. and Celarier, E. A.: Earth surface reflectivity climatology at 340–380 nm from EP-TOMS data, *J. Geophys. Res.*, 102, 28003–28011, 1997.
- Herman, J. R., Krotkov, N., Celarier, E., Larko, D., and Labow, G.: Distribution of UV radiation at the Earth's surface from TOMS-measured UV-backscattered radiances, *J. Geophys. Res.*, 104, 12059–12076, doi:10.1029/1999JD900062, 1999.
- Herman, J. R.: Global increase in UV irradiance during the past 30 years (1979–2008) estimated from satellite data, *J. Geophys. Res.*, 115, D04203, doi:10.1029/2009JD012219, 2010.
- Herman, J. R., Labow, G., Hsu, N. C., and Larko D.: Changes in cloud and aerosol cover (1980–2006) from reflectivity time series using SeaWiFS, N7-TOMS, EP-TOMS, SBUV-2, and OMI radiance data, *J. Geophys. Res.*, 114, D01201, doi:10.1029/2007JD009508, 2009.
- HIRLAM – High Resolution Limited Area Model: The International Satellite Cloud Climatology Project (ISCCP) <http://isccp.giss.nasa.gov/index.html>, last access: 6 December 2012.
- Kalliskota, S., Kaurola, J., Taalas, P., Herman, J., Celarier, E., and Krotkov N. A.: Comparison of daily UV doses estimated from Nimbus-7/EPTOMS measurements and ground-based spectroradiometric data, *J. Geophys. Res.*, 105, 5059–5062, 2000.
- Kazadzis, S., Bais, A., Arola, A., Krotkov, N., Kouremeti, N., and Meleti, C.: Ozone Monitoring Instrument spectral UV irradiance products: comparison with ground based measurements at an urban environment, *Atmos. Chem. Phys.*, 9, 585–594, doi:10.5194/acp-9-585-2009, 2009.
- Kazantzidis, A., Bais, A. F., Gröbner, J., Herman, J. R., Kazadzis, S., Krotkov, N., Kyro, E., den Outer, P. N., Garane, K., Gorts, P., Lakkala, K., Meleti, C., Slaper, H., Tax, R. B., Turunen, T., and Zerefos, C. S.: Comparison of satellite-derived UV irradiances with ground-based measurements at four European stations, *J. Geophys. Res.*, 111, D13207, doi:10.1029/2005JD006672, 2006.
- Kleipool, Q. L., Dobber, M. R., de Haan, J. F., and Levelt, P. F.: Earth surface reflectance climatology from 3 years of OMI data, *J. Geophys. Res.*, 113, D18308, doi:10.1029/2008JD010290, 2008.
- Krotkov, N. A., Herman, J. R., Bhartia, P. K., Fioletov, V., and Ahmad, Z.: Satellite estimation of spectral surface UV irradiance, 2. Effects of homogeneous clouds and snow, *J. Geophys. Res.*, 106, 11743–11759, 2001.
- Labow, G. J., Herman, J. R., Huang, L.-K., Lloyd, S. A., DeLand, M. T., Qin, W., Mao, J., and Larko, D. E.: Diurnal variation of 340 nm Lambertian equivalent reflectivity due to clouds and aerosols over land and oceans, *J. Geophys. Res.*, 116, D11202, doi:10.1029/2010JD014980, 2011.
- Levelt, P. F., van den Oord, G. H. J., Dobber, M. R., Mälkki, A., Visser, H., de Vries, J., Stammes, P., Lundell J., and Saari, H.: The Ozone Monitoring Instrument, *IEEE T. Geosci. Remote. Sens.*, 44, 1093–1101, doi:10.1109/TGRS.2006.872333, 2006.
- Lindfors, A., Tanskanen, A., Arola, A., van der A, R., Bais, A. F., Feister, U., Janouch, M., Josefsson, W., Koskela, T., Lakkala, K., den Outer, P. N., Smedley, A. R. D., Slaper, H., and Webb, A. R.: The Promote UV Record: toward a global satellite-based climatology of ultraviolet irradiance, *IEEE-J. Sel. Top. Appl. Earth Obs.*, 2, 207–212, doi:10.1109/JSTARS.2009.2030876, 2009.
- Matthijsen, J., Slaper, H., Reinen, H. A. J. M., and Velders, G. J. M.: Reduction of solar UV by clouds: A comparison between satellite-derived cloud effects and ground-based radiation measurements, *J. Geophys. Res.*, 105, 5069–5080, doi:10.1029/1999JD900937, 2000.
- McKinley, A. and Diffey, B. L.: A reference action spectrum for ultra-violet induced erythema in human skin, in: Human Exposure to Ultraviolet Radiation: Risks and Regulations, *Int. Congr. Ser.*, edited by: Passchier, W. F. and Bosnjakovich, B. F. M., Elsevier, New York, 83–87, 1987.
- Slaper, H., Reinen, H. A. J. M., Blumthaler, M., Huber, M., and Kuik, F.: Comparing groundlevel spectrally resolved UV measurements from various instruments: a technique resolving effects of wavelengthshifts and slitwidths, *Geophys. Res. Lett.* 22, p. 2721, 1995.
- Tanskanen, A., Lindfors, A., Määttä, A., Krotkov, N., Herman, J., Kaurola, J., Koskela, T., Lakkala, K., Fioletov, V., Bernhard, G., McKenzie, R., Kondo, Y., O'Neill, M., Slaper, H., den Outer, P., Bais, A. F., and Tamminen, J.: Validation of daily erythemal doses from Ozone Monitoring Instrument with ground-based UV measurement data, *J. Geophys. Res.*, 112, D24S44, doi:10.1029/2007JD008830, 2007.
- UNEP: Environmental effects of ozone depletion and its interaction with climate change: 2010 assessment, 278, United Nations Environmental Programme (UNEP), Nairobi, 2010.
- Van Dijk A., den Outer, P. N., and Slaper, H.: Climate and ozone change effects on ultraviolet radiation and risks (COEUR). Using and validating earth observation, RIVM Report 610002001, www.rivm.nl/bibliotheek/rapporten/610002001.pdf (last access: 6 December 2012), 2008.

van der A, R. J., Allaart, M. A. F., and Eskes, H. J.: Multi sensor re-analysis of total ozone, *Atmos. Chem. Phys.*, 10, 11277–11294, doi:10.5194/acp-10-11277-2010, 2010.

Williams, J. E., den Outer, P. N., Slaper, H., Matthijssen, J., and Kelfkens, G.: Cloud induced reduction of solar UV-radiation: A comparison of ground-based and satellite based approaches, *Geophys. Res. Lett.*, 31, L03104, doi:10.1029/2003GL018242, 2004.

WMO – World Meteorological Organization: Scientific Assessment of Ozone Depletion: 2010, Global ozone Research and Monitoring Project – Report No. 52, 438, World Meteorological Organisation, Geneva, Switzerland 2011.